

Leveraging Scale-aware Representations for improved Concept-Representation Alignment in ViTs

Sanchit Sinha¹, Guangzhi Xiong¹ and Aidong Zhang¹

¹University of Virginia

{sanchit, hhu4zu, aidong}@virginia.edu,

Abstract

Vision Transformers (ViTs) are increasingly being adopted in various sensitive vision applications - like medical diagnosis, facial recognition, etc. To improve the interpretability of such models, many approaches attempt to *forward-align* them with carefully annotated abstract, human-understandable semantic entities - **concepts**. Concepts provide *global rationales* to the model predictions and can be quickly understood/intervened on by domain experts. Most current research focuses on designing model-agnostic, plug-and-play generic concept-based explainability modules that do not incorporate the inner workings of foundation models (e.g., inductive biases, scale invariance, etc.) during training. To alleviate this issue for ViTs, in this paper, we propose a novel Concept Representation Alignment Module (CRAM) which learns both scale and position-aware representations from multi-scale feature pyramids and patch representations respectively. CRAM further aligns these representations with concept annotations through an attention matrix. The proposed CRAM module improves the predictive performance of ViT architectures and also provides accurate and robust concept explanations as demonstrated on five datasets - including three widely used benchmarks (CUB, Pascal APY, Concept-MNIST) and 2 real-world datasets (AWA2, KITS).

1 Introduction

With the surge of advanced deep learning (DL) methods, deep neural networks (DNNs), especially Transformer-based networks [Vaswani *et al.*, 2017], have been widely deployed in human communities for the benefit of our life [Dargan *et al.*, 2020; Shorten *et al.*, 2021]. Research in developing high-performing, generalizable, and efficient architectures has led to experts classifying a family of fundamental architectures as ‘Foundation Models’ [Bommasani *et al.*, 2021]. In computer vision, the most widely utilized foundation model, Vision Transformers (ViT), shows great scalability and impressive performance in various downstream tasks, which promotes its use in real-world applications like autonomous driving [Ando

et al., 2023; Dong *et al.*, 2021]. However, with the development and application of such advanced DNNs, there is a growing concern about their lack of interpretability and hesitation in applying the technology in high-stakes areas such as medical diagnosis, facial recognition, finance, etc. Given the current situation, a number of studies on the interpretability of DNNs have emerged [Li *et al.*, 2022].

Current research on DNN interpretability can be broadly categorized into two classes dubbed **backward and forward** alignment [Gabriel, 2020]. *Backward* alignment is post-hoc interpretation, which explains already trained models. Specifically, some post-hoc methods assign relative importance scores to different features considered [Ribeiro *et al.*, 2016; Sundararajan *et al.*, 2017], while some other approaches will rank the input training samples according to their importance to prediction [Koh and Liang, 2017; Ghorbani and Zou, 2019]. *Forward* alignment methods try to design and train intrinsically interpretable models. For example, various approaches have attempted to incorporate human-understandable concepts into model architecture and training processes. Concepts can be considered as shared abstract entities across multiple instances, which provide a general understanding of the task processed by the model. Many studies have explored how to integrate the model’s decision-making process with task-relevant concepts to achieve transparent, interpretable model predictions [Koh *et al.*, 2020; Pedapati *et al.*, 2020; Jeyakumar *et al.*, 2020; Heskes *et al.*, 2020; O’Shaughnessy *et al.*, 2020; Kim *et al.*, 2018; Li *et al.*, 2018; Alvarez Melis and Jaakkola, 2018; Chen *et al.*, 2019]. Formally, given a set of concept representations C associated with an input sample x , the task prediction is $y = g(C)$, where g is any interpretable function used to aggregate concepts. Multiple works such as [Alvarez Melis and Jaakkola, 2018] and [Agarwal *et al.*, 2021] have postulated using a weighted linear sum of concepts as g . Other works such as [Koh *et al.*, 2020] have postulated using a shallow feed-forward network as mapping from concepts to prediction.

With the success of attention mechanism [Vaswani *et al.*, 2017] in designing large-scale networks for language [Devlin *et al.*, 2018] and vision applications [Dosovitskiy *et al.*, 2020], multiple diverse use-cases for attention have been proposed. A particular use case of attention in concept-based explainability is utilizing the attention mechanism in modeling the concept aggregation function g as first proposed in [Rig-

otti *et al.*, 2021]. Note that concepts are independent entities shared among different training samples, hence attention can be reliably used to assign “relevance” scores to the concepts relative to a prediction.

ViTs [Dosovitskiy *et al.*, 2020] demonstrate significant improvement over traditional models like CNNs for large-scale vision applications. ViTs borrow their architecture from transformer-based language approaches [Vaswani *et al.*, 2017; Devlin *et al.*, 2018]. A ViT first segments an image into equal patches, which are projected into an embedding space with positional information. The representation is then passed through stacked transformer blocks which is used in downstream tasks. ViTs have demonstrated better performance than CNNs, especially when pre-trained with large-scale data. However, due to the very architecture of ViTs being borrowed from language paradigm, they lack vision-specific *inductive biases*. CNNs, which have been specifically designed for image modalities, capture explicit inductive biases such as - scale invariance and transformation equivariance. As an example, ViTs are demonstrated not to be scale-insensitive [Xu *et al.*, 2021], a known strength of CNNs. Researchers have attempted to improve ViTs by incorporating CNN-like inductive biases in their architectures with great success [Liu *et al.*, 2021; Graham *et al.*, 2021]. Concept-based explainability approaches are usually designed to be model-agnostic [Koh *et al.*, 2020] and plug-and-play [Rigotti *et al.*, 2021] to fit all possible use cases. However, as discussed, a detailed and nuanced consideration should be incorporated while designing concept-based explainability modules as well. As a consequence, we augment present attention-based concept explainability modules with multi-scale features to improve the alignment of model representations with concepts, thus incorporating desirable properties (inductive biases) of both ViTs and CNNs in our proposed module.

In this paper, we propose **Attention-based Concept Alignment Module (ACAM)**, a concept-based explainability module for ViTs to *align* human-annotated concepts with model representations. Unlike model-agnostic plug-and-play explainability, ACAM effectively composes inductive biases of CNNs and ViTs - scale invariance and image-patch relationship awareness respectively into scale and patch-aware representations. More precisely, ACAM consists of 3 distinct modules - (i) **Multi-scale Encoding (MSE) Module**, which models concepts at various scales, (ii) **Deformable Multi-Scale Fusion (DMSF) Module**, which composes multi-scale concepts with patch embeddings, and (iii) **Concept-Representation Alignment Module (CRAM)**, which aligns concepts with the learned model representations. To summarize, our contributions are:

- We propose ACAM, a concept-based explainability module that effectively composes inductive biases from CNNs and ViTs to perform better model representation-concept alignment.
- We demonstrate through quantitative experiments that ACAM improves both prediction accuracy and reduces concept-learning errors as compared to model-agnostic attention-based concept explainability modules across 7

different vision-transformer architectures.

- We demonstrate through diverse real-world visual examples that ACAM captures concept annotations missed by model-agnostic modules and is robust to simple transformations and perturbations.

2 Related Work

Vision Transformers (ViTs) and Inductive biases. Multiple approaches have improved the original ViT [Dosovitskiy *et al.*, 2020] performance [Atito *et al.*, 2021; Gong *et al.*, 2021], efficiency [Chen *et al.*, 2022] and explainability [Xu *et al.*, 2023]. Even though ViTs offer better downstream task performance as compared to CNN-centric approaches [Tuli *et al.*, 2021; Raghu *et al.*, 2021], the consensus among researchers remains that ViTs have much less stringent inductive biases and some approaches improve them [Xu *et al.*, 2021]. To alleviate this problem, namely - lack of scale invariance and transform equivariance, DETR [Zhu *et al.*, 2020] proposes an attention mechanism to incorporate scale features while SWIN [Liu *et al.*, 2021] uses a shifted window approach in ViTs with great success.

Concept-based Explainability and Attention. Concept-based explanations explain models using human-understandable concepts [Koh *et al.*, 2020; Jeyakumar *et al.*, 2020; Kim *et al.*, 2018; Sinha *et al.*, 2024]. Concepts are high-level attributes that are shared across different instances [Chen *et al.*, 2019; Koh *et al.*, 2020]. Various explorations uncover the decision-making of black-box neural networks via concepts, including learning latent concept scores [Alvarez Melis and Jaakkola, 2018], finding concept prototypes [Li *et al.*, 2018; Chen *et al.*, 2019], and checking concept activations [Kim *et al.*, 2018].

Comparison with related approaches. Recent approaches incorporate an external Attention matrix to align model representations with human-understandable concepts. The closest works to our method ACAM are - Concept Bottleneck Models (CBMs) [Koh *et al.*, 2020], CT [Rigotti *et al.*, 2021], and BotCL [Wang *et al.*, 2023]. Both CBMs and BotCL utilize an intermediate layer to perform alignment between concepts and representations but neither utilize spatial concept annotation maps - CBMs discretize the concepts to binary labels while BotCL is completely unsupervised and utilizes slot attention to learn representative concepts. Even still, we still compare performance against CBMs. The closest work to ACAM is CT [Rigotti *et al.*, 2021] which utilizes a model-agnostic plug-and-play module to align concepts with representations. However, there are significant differences between our approach and CT. Firstly, their module is model-agnostic and does not account for the inductive biases. Secondly, their method does not incorporate the effect of scale - making it fragile to minor transformations. Finally, their method does not provide any analysis on its effectiveness over ViT scale and architecture - a very important determinant of the extent of misalignment.

3 Methodology

In this section, we introduce our proposed *Attention-based Concept Alignment Module (ACAM)*. ACAM is composed of

three independent sub-modules, namely - the Multi-scale encoding (MSE) module which extracts multi-scale features for enhanced scale awareness, the Deformable Multi-Scale Fusion (DMSF) Module which incorporates image scales using Deformable Attention, and the Concept-Representation Alignment Module (CRAM) which aligns scale and patch aware features with concept annotations. The ACAM module can be utilized as a classification head on top of standard ViT backbones for improved concept-based explanations. The overall schematic representation of the ACAM module is shown in Figure 1.

Problem Setting: A concept-based model consists of networks f and g . For a given training sample $\{(x_i, y_i, C_i)\}$, where $x_i \in \mathbb{R}^D$ denotes the i -th training sample, $y_i \in \mathbb{R}$ is the target classification label for sample x_i , and $C_i \in \mathbb{R}^T$ is a vector of T human annotated concepts, the network f learns a mapping from image space to the concept space, i.e., $f: \mathbb{R}^D \rightarrow \mathbb{R}^T$, while the network g maps concepts to the prediction space, i.e., $g: \mathbb{R}^T \rightarrow \mathbb{R}$. The training procedure entails supervising the concept space with human-annotated concepts and promoting the alignment of concepts and model representations. In our method, the concepts C_i are the annotated concept maps with pixel-level annotations.

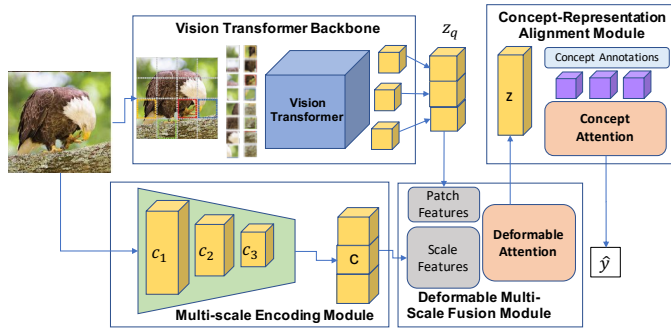


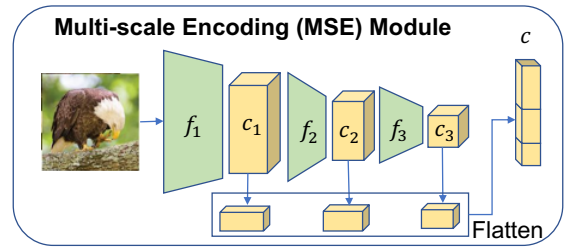
Figure 1: Schematic overview of the proposed ACAM module. Given an input image, the Multi-scale encoding (MSE) module encodes representations at various scales in \mathbf{c} . Patch-aware representations \mathbf{z}_q from the ViT are composed using the Deformable Multi-Scale Fusion (DMSF) Module. The Concept-Representation Alignment Module (CRAM) aligns the learned representations \mathbf{z} with concept annotations C . \hat{y} is the model estimation of the true task label y .

3.1 Multi-scale encoding Module

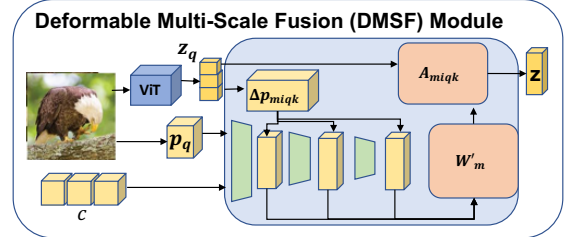
The Multi-scale encoding Module consists of a Convolutional Neural Network (CNN) \mathbf{F} which can be thought of as S stacked convolution blocks (with implicit activation and pooling operations) f_i , such that $\mathbf{F} = f_S \circ f_{S-1} \circ f_{S-2} \dots \circ f_1$. CNNs embody inductive biases in the form of convolution operations which capture the *local semantics* of images at various scales, i.e., each block computes feature maps representing various scales. As a consequence, for a given input image $x \in \mathbb{R}^D$, we extract S multiscale features from various blocks of \mathbf{F} . Mathematically, each feature for a particular scale can be computed as

$$c_i = f_i \circ f_{i-1} \dots \circ f_1(x), i \in \{1, \dots, S\} \quad (1)$$

Subsequently, the combined multiscale features are concatenated by the MSE module to output a combined and spatially



(a) The Multi-scale encoding (MSE) Module.



(b) The Deformable Multi-Scale Fusion (DMSF) Module.

Figure 2: (a) Detailed view of the MSE module which extracts multi-scale features $\{c_i\}_1^S$ and concatenates them together into a vector \mathbf{c} . (b) Detailed view of the proposed DMSF module utilizing Deformable Attention operation to combine multi-scale features \mathbf{c} with patch embeddings from ViT (\mathbf{z}_q) to output scale and patch-aware representations \mathbf{z} .

aware multi-scale feature \mathbf{c} . Mathematically, the scale-aware feature \mathbf{c} is given as,

$$\mathbf{c} = \{\text{flatten}(c_1), \text{flatten}(c_2), \dots, \text{flatten}(c_S)\} \quad (2)$$

Note that the feature \mathbf{c} is sometimes called the feature pyramid [Lin *et al.*, 2017; Chen *et al.*, 2022] because it intuitively represents multiple scales of the same image, each scale progressively smaller than the previous scale. The architecture of the MSE module is presented in Fig. 2 (a).

3.2 Deformable Multi-Scale Fusion Module

The DMSF module consists of two distinct steps. The first step computes an attention operation using deformed (scaled) outputs \mathbf{c} from the MSE module with the Multi-Scale Deformable Attention (MSDA) operation [Zhu *et al.*, 2020] as discussed below. The second step composes a list of patch outputs \mathbf{z}_q from a ViT backbone with multi-scale features computed from the MSDA operation using a combination of a learnable parameter (\mathbf{I}) and a tunable hyperparameter (ψ).

Multi-scale Deformable Attention (MSDA) Operation. As discussed before, the fundamental problem in the standard attention mechanism used in ViTs is the lack of scale and spatial awareness. To incorporate multi-scale feature maps, Zhu *et al.* [2020] proposed MSDA. The MSDA operation is characterized by a set of reference points (depicted by coordinates \mathbf{p}_q) shared among features corresponding to multiple scales of the same image's feature maps which localizes semantics across scales. Mathematically, the MSDA operation for a set of feature-maps of various scales $\{c_i\}_1^S$ over a query-sample

\mathbf{z}_q , the $MSDA(\mathbf{z}_q, \mathbf{p}_q, \mathbf{c})$ operation can be represented as,

$$\sum_{m=1}^M \mathbf{W}_m \left[\sum_{i=1}^S \sum_{k=1}^K \mathbf{A}_{miqk} \cdot \mathbf{W}'_{m c_i} (\phi_i(\mathbf{p}_q) + \Delta \mathbf{p}_{miqk}) \right] \quad (3)$$

where M represents the number of attention heads, S represents the number of scales, K represents the number of sampled reference points, \mathbf{W} represents a projection to multiple heads for the Value vector, \mathbf{A} represents the attention matrix, and $\Delta \mathbf{p}_{miqk}$ represents offset corresponding to sampled reference points \mathbf{p}_q (see detail on \mathbf{p}_q in [Zhu *et al.*, 2020]). Correspondingly, each element in \mathbf{A} is referenced as head (m), each scale (i), q and k represent the query and key indices. As a consequence, the number of reference points sampled is $S * K$. The function ϕ scales up/down the reference points to corresponding scales as c_i . Intuitively, the module can be understood as utilizing multi-scale features as key/value vectors which transform a non-scale-aware query vector (\mathbf{z}_q) into a scale-aware query vector (\mathbf{z}).

Adaptive Patch Composition. Note that the output from the ViT backbone is represented as \mathbf{z}_q (Figure 1), which is treated as the query vector for the MSDA operation. Even though the MSDA operation introduces scale awareness in the outputs of the ViT backbone, a tradeoff between patch-specific semantics and scale awareness is desirable due to the wide gulf in the inductive biases in them. To alleviate this, we introduce a learnable vector \mathbf{I} which controls the contribution of scale features, and a scalar hyperparameter ψ which weighs the effect of the MSDA operation on the final patch vector. Mathematically, the final output of the DMSF module is given as follows

$$\mathbf{z} = \text{norm}(\mathbf{z}_q + \psi \cdot \mathbf{I} \cdot MSDA(\mathbf{z}_q, \mathbf{p}_q, \mathbf{c})) \quad (4)$$

where norm represents the layer norm, \mathbf{z}_q represents the input from the ViT backbone, \mathbf{p}_q represents the reference points while $\mathbf{c} = \{c_i\}_1^S$ represents the multi-scale features computed by the MSE module. Note that adaptive composition is sensitive to the initialization of the \mathbf{I} vector and the tunable hyperparameter ψ . An overview of the DMSF module is shown in Fig. 2 (b).

3.3 Concept-Representation Alignment Module

The Concept-Representation Alignment Module (CRAM) is inspired by the Attention mechanism proposed in Vaswani *et al.* [2017] for better concept alignment. Recall that an attention matrix \mathbf{A} computation is conditioned on three vectors of the same dimensions - Query (Q), Key (K), and Value (V). Mathematically, the attention operation is as follows:

$$\text{Att}(Q, K, V) = \text{softmax}\left(\frac{QK^T}{\sqrt{\text{dim}}}\right)V = \mathbf{A}\mathbf{V} \quad (5)$$

The attention matrix attends to each value in the Query and Key vectors with a composite score. CRAM treats the Query vector as the patch representation \mathbf{z} from the DMSF module and the Key Vector as Human-annotated Concepts C . As patches and concepts are continuous and one-hot respectively, projection matrices convert them to continuous vectors. Mathematically, the attention matrix for patch embeddings (\mathbf{z}) and concepts (C) associated to an input sample x is

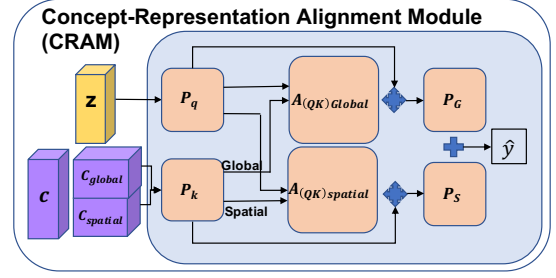


Figure 3: Detailed view of the Concept-Representation Alignment Module (CRAM). CRAM aligns scale and patch-aware representations (\mathbf{z}) and human-annotated concepts (C). The matrices P_q , P_k and P_{v1}, P_{v2} are projection matrices while $\mathbf{A}_{\text{Spatial}}$ and $\mathbf{A}_{\text{Global}}$ are attention matrices between concept projections and patch embedding projections. The final prediction \hat{y} is the average of outputs between spatial and global attention operations.

calculated as follows:

$$\mathbf{A}_{QK} = \text{softmax}\left(\frac{(\mathbf{z}P_q)(CP_k)^T}{\sqrt{\text{dim}}}\right) \quad (6)$$

where the matrices P_q and P_k are learnable projection matrices transforming patches and concepts to Query and Key vectors respectively, while dim represents the dimension of the patch and concept embeddings. Intuitively, each entry in the matrix \mathbf{A}_{QK} encapsulates the contribution of a concept on a patch and is a measure of alignment. The final prediction is then calculated by multiplying the attention matrix with concept projections ($V = CP_k$) followed by a final learnable projection matrix (P_v) to map to logits. Mathematically each logit \hat{y} in the prediction \hat{y} can be calculated as an average of concept contributions on each patch.

$$\hat{y} = \frac{1}{|\mathbf{z}|} \sum_{|\mathbf{z}|} \mathbf{A}_{QK} V P_v \quad (7)$$

where $|\mathbf{z}|$ stands for the dimension of \mathbf{z} . In practice, two different attention matrices ($\mathbf{A}_{\text{Spatial}}$ and $\mathbf{A}_{\text{Global}}$ - the QK subscript is omitted for clarity) are calculated for different subsets of concepts - spatial and global (Refer to Appendix). The spatial concepts can be localized, while the global concepts are more semantic and cannot be localized. The final output is then the sum of logits computed from both spatial and global attention matrices. Mathematically the sum can be written as

$$\hat{y} = \frac{1}{|\mathbf{z}|} \sum_{|\mathbf{z}|} \mathbf{A}_{\text{Spatial}} V P_{v1} + \frac{1}{|\mathbf{z}|} \sum_{|\mathbf{z}|} \mathbf{A}_{\text{Global}} V P_{v2} \quad (8)$$

where P_{v1} and P_{v2} are different versions of P_v associated with $\mathbf{A}_{\text{Spatial}}$ and $\mathbf{A}_{\text{Global}}$, respectively. The detailed description of CRAM is shown in Figure 3.

3.4 End-to-end Training of ViT with ACAM

The overall schematic pipeline of our approach is depicted in Figure 1. As MSE, DMSF and CRAM modules are standalone modules that can be appended on top of any standard ViT backbone. To sum up, the inference step for an input

image x utilizing ACAM computes the patch embeddings \mathbf{z}_q through the following procedure:

$$\hat{y} = \text{CRAM}(\mathbf{z}, C), \text{ where } \mathbf{z} = \text{DMSF}(\mathbf{z}_q, \mathbf{c}), \mathbf{c} = \text{MSE}(x) \quad (9)$$

Training Objective. The final training objective includes the task prediction objective utilizing a classification loss. For datasets with explicit localization of concepts in the image (e.g. CUB), the attention matrix $\mathbf{A}_{\text{Spatial}}$ can be regularized by human-annotated localizations. Mathematically, the training objective can be given as:

$$\mathcal{L}_{\text{ACAM}} = \mathcal{L}(\hat{y}, y) + \lambda \|\mathbf{A}_{\text{Spatial}} - H\|_F \quad (10)$$

where \mathcal{L} represents any classification loss, H denotes human-annotated localization points for the concepts, λ is a tunable hyperparameter and the subscript F is the Frobenius norm.

4 Experiments and Results

4.1 Dataset Description

- **CUB200** [Wah *et al.*, 2011]: The Caltech-UCSD Birds-200-2011 dataset consists of 11,788 photos of 200 different classes of birds annotated with concepts representing physical traits of birds like wing color, beak size, etc.
- **AWA2** [Xian *et al.*, 2018]: Animals with Attributes-2 consists of 37,322 images of a combined 50 animal classes with 85 binary concepts like number of legs, presence of tail, etc. We utilize Segment Anything Model (v2)¹ to annotate 10 selected concepts.
- **Kidney Tumor Segmentation** [Heller *et al.*, 2023]: The KITS challenge dataset consists of images of kidneys where the task is segmentation of renal cysts and tumors. We augment each image with the concepts from the meta-data, namely - kidney, tumor, and cysts. We sample 10000 images with an 80:20 train/test split.
- **PascalAPY** [Farhadi *et al.*, 2009]: We utilize Pascal Object Recognition Dataset as processed and described in [Rigotti *et al.*, 2021]. After processing, it consists of 14350 images with 20 attributes each.
- **C-MNIST** [Sinha *et al.*, 2023]: Concept-MNIST entails augmenting MNIST dataset with two “spatial” concepts in the form of curved and straight lines. We consider two tasks - even/odd and digit classification.

4.2 Baselines and Evaluation Metrics

Comparison Baselines. As discussed in Related Work, our method is the first to utilize inductive biases in attention-based concept explainability. The closest comparison to our method is CBM [Koh *et al.*, 2020] (CBMs do not utilize concept attention maps, only global concepts) and Rigotti *et al.* [2021] which only utilizes an inferior attention-only architecture similar to only a CRAM module. **We denote [Rigotti *et al.*, 2021] as “Only CRAM”.** We compare our approach on a variety of ViT baselines - with ViT-Base, ViT-Large [Dosovitskiy *et al.*, 2020], SWIN [Liu *et al.*, 2021] for all datasets. ViT-Base and ViT-Large are chosen to demonstrate the effect

of scale awareness, while SWIN is chosen to demonstrate the effect of inductive bias in the backbone. In addition, we also compare the CUB dataset on DeIT [Touvron *et al.*, 2021], ViT-Base (Dino) [Caron *et al.*, 2021]. SWIN incorporates inductive biases from CNNs. Dino is a robustly trained ViT while DeIT is a distilled version, further capturing the diversity in training procedures.

Evaluation Metrics. The evaluation metric for task prediction is accuracy across all five datasets. For datasets with spatial concept annotations - namely CUB, AWA2, and KITS, we utilize the Pixel True Positive Rate (Px. TPR) which measures the percentage of correctly identified concept annotations. Due to the extremely precise and sensitive setting of KITS dataset, we measure the total pixel accuracy which encompasses both accurately identified concept and non-concept pixels. For datasets with no spatial concept annotations (only global) - namely C-MNIST and Pascal APY, we utilize 0-1 error (misclassification) for concepts as only binary concepts are considered. Additionally, for CUB200, as localization information for each concept is present, the concept errors are directly evaluated with the Frobenius norm of the difference between ground truth annotations and predicted concept attention matrices (Appendix).

4.3 Implementation Details

ViT Backbone. We set the patch size to correspond to 16x16 pixels. Each image is resized to (224,224), hence a patch sequence is $(224/16, 224/16) = (14,14)$. Following Rigotti *et al.* [2021], we append the <CLS> token to the patch sequence after positional embeddings encapsulating global semantics. This results in an input sequence of length of $196+1 = 197$ tokens. The internal embedding size (dim) of ViT is 1024.

MSE Module. We utilize three scales in the Multi-scale encoding Module, i.e., $S = 3$. We utilize scales - 1/8, 1/16, and 1/32 corresponding to scale-aware vector \mathbf{c} composed of sizes: $c_1 = 1024$, $c_2 = 196$ and $c_3 = 16$, making the size of $\mathbf{c} = 1029$. The first convolution block consists of three convolution layers with batch-norm followed by Max pooling. The following convolution blocks consist of a single convolution layer of kernel size=3 and stride=2 with batch norm.

DMSF Module. We utilize Multi-scale Deformable Attention [Zhu *et al.*, 2020]. We utilize 16 attention heads and four reference points, along with layer norms for each key, query, and value vector. We strip <CLS> token before passing through the DMSF module and append it to the output. The initialization value of \mathbf{I} is set as 0.01. The value of ψ is tunable and set as 1 for CUB, 2 for Concept-MNIST and Pascal aPY, and 0.5 for AWA2 and KITS.

CRAM Module. We utilize the same embedding dimensions, i.e., $dim = 1024$ for Key, Query and Value vectors. The number of attention heads is set as 2 for both global and spatial concept attention matrices. (Appendix)

Training Details. We train each dataset and backbone for 50 epochs with early stopping. The maximum learning rate is set at $5e-5$ with a linear warmup for the first 10 epochs followed by Cosine decay. The batch size is 16 for each dataset with mixed precision (16-bit default) optimization.

¹<https://github.com/facebookresearch/sam2>

Head	Backbone	CUB200		AWA2		KITS	Concept-MNIST		Pascal aPY
		Accuracy	Px. TPR	Accuracy	Px. TPR	Px. Acc.	Class.	Odd/Even	Accuracy
CBM	ViT-Large	81.03	-	53.14	-	-	93.83	97.12	81.1
CRAM (CT)	ViT-Base	84.41 ± 0.3	82.25 ± 0.32	62.3 ± 0.2	64.02 ± 0.56	91.89 ± 2.45	95.71 ± 0.1	97.58 ± 0.1	81.0 ± 0.8
	ViT-Large	86.31 ± 0.2	83.55 ± 1.14	63.6 ± 0.1	68.04 ± 1.44	94.33 ± 2.03	95.74 ± 0.1	97.94 ± 0.1	81.3 ± 0.8
	SWIN	85.71 ± 0.1	82.28 ± 0.83	62.3 ± 0.1	67.84 ± 0.75	92.81 ± 1.87	94.83 ± 0.1	97.68 ± 0.1	81.3 ± 0.8
ACAM	ViT-Base	85.71 ± 0.3	83.93 ± 0.21	62.3 ± 0.1	64.11 ± 1.21	92.33 ± 0.87	95.83 ± 0.1	97.91 ± 0.1	81.4 ± 0.8
	ViT-Large	87.26 ± 0.3	87.21 ± 0.97	63.7 ± 0.1	73.12 ± 0.39	95.84 ± 1.89	95.83 ± 0.1	97.91 ± 0.1	81.9 ± 0.8
	SWIN	85.74 ± 0.1	83.41 ± 1.33	62.5 ± 0.4	69.66 ± 0.44	93.02 ± 1.35	94.83 ± 0.1	97.91 ± 0.1	81.4 ± 0.8

Table 1: We report Accuracy and True Positive Rate (TPR) for CUB200 and AWA2 datasets, over backbones ViT-Base, ViT-Large, and SWIN augmented with CRAM (Rows 2-4) and ACAM augmented backbones (Rows 5-7). For the KITS dataset, we report the total pixel accuracy. For Concept-MNIST, we report accuracy on two tasks - Digit classification and Odd/Even detection; for Pascal aPY, we report both accuracy on object detection task. Refer to Appendix for details on task settings. All results are averaged over 3 seeds, and std dev is reported.

4.4 Quantitative Results

Task Prediction Performance.

Table 1 reports the task prediction performance across all five datasets with ViT backbones using CBM (Row-1), augmented with only CRAM (Rows 2-4) and ACAM module (Rows 5-7). Rows 2-4 list the prediction performance of backbones augmented with only the CRAM module on - ViT-Base, ViT-Large, and SWIN. Rows 5-7 list the performance on the same architectures using ACAM. ACAM outperforms CBMs and only CRAM on all datasets. Interestingly, on SWIN backbones the performance of ACAM and ‘only CRAM’ is on par - implying that SWIN captures scale inductive biases better than ViTs but performs worse than ViT-Large (a larger model). These results demonstrate that both size and inductive biases of ViTs are important factors in improving prediction and concept performances. Our module is effective in introducing scale awareness in standard ViTs and improving their performance.

Concept Annotation Performance.

As concept performance metrics are different for datasets with spatial concept annotations and global annotations, we discuss the results individually.

True Positive Rate (TPR): For CUB200 and AWA2, we observe that pixel-wise TPR improves by $\sim 4\%$ on CUB200 and $\sim 5\%$ implying that ACAM captures pixels of interest much better than only CRAM. In Fig 6, we demonstrate the effect on random test images where ACAM captures concept annotations more effectively than only CRAM.

Pixel Accuracy: For KITS, we report total pixel accuracy which includes both concept and background annotations. Note that due to the sensitive nature of KITS, it is important to correctly identify both relevant concepts (cysts) and irrelevant ones (kidney surface). We observe that ACAM outperforms only CRAM by $\sim 1.5\%$ over all ViT architectures on KITS.

Misclassification Errors (Appendix) For datasets with only global concepts and no spatial annotations, we report the 0-1 concept error i.e. misclassification. We observe that ACAM outperforms only CRAM on both C-MNIST and Pascal aPY.

4.5 Ablation Studies

Hyperparameter Ablations.

We demonstrate the effect of the most important hyperparameters in the DMSF module in Figure 4. For all experiments, a ViT-Base model is utilized and trained on the CUB dataset. Figure 4a demonstrates the effect of increasing the number of

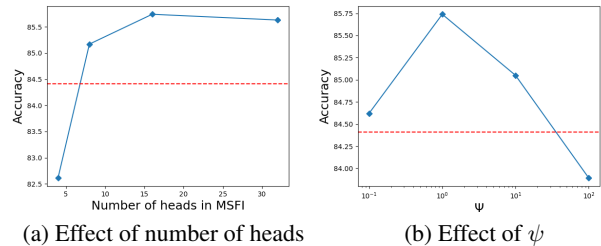


Figure 4: Effect of most relevant hyperparameters - attention heads and ψ in the DMSF module on performance. The dotted red line shows the baseline performance of utilizing only CRAM.

attention heads on the prediction performance. We observe that the increased number of attention heads improves performance by attending to various scales effectively. However, the maximum performance is observed at 16 heads implying that too many heads might result in the model focusing on non-relevant parts. Next, Figure 4b demonstrates the predictive performance as a function of increasing values of ψ (i.e., increasing weight of scale-aware features on \mathbf{z}). Here, we observe that a tradeoff exists between ψ and predictive performance. The reason for this behavior is with higher ψ , scale-aware inductive biases begin dominating the patch embeddings and the performance gravitates towards being similar to models with high CNN-like inductive biases (Table 1).

Modules	Concept-MNIST		CUB200	AWA2
	Odd/Even	Class.	Class.	Class.
ViT-base	97.12	93.82	82.91	61.7
w/ CRAM	97.78	95.71	84.41	62.1
w/ CRAM+MSE	97.87	95.65	85.17	62.7
ACAM	97.88	95.84	85.73	63.4

Table 2: Task prediction performance ablating on proposed modules of ACAM over a single run. ‘Class.’ refers to Classification task. NOTE: ACAM implies Backbone w/ MSE+DMSF+CRAM.

Module Ablations.

Next, we progressively demonstrate each submodule’s effect in Table 2. Line-1 lists the performance of ViT-base with no concept information. Next, Line-2 lists the performance only using the CRAM module. Line-3 lists the performance with both the MSE and CRAM modules. As we observe, adding scale-aware features indeed improves performance. The last line (Line-5) lists performance when the DMSF module performs feature fusion - performing the best.

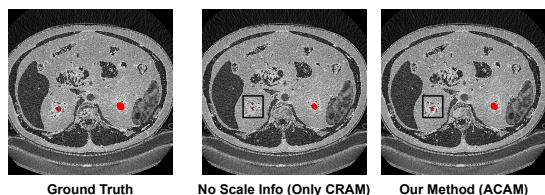


Figure 5: Effect of Scale: Visualized concept annotations for a correctly classified sample from KITS. As seen, ACAM identifies the small ‘cyst’ annotation much more accurately (Acc = 91.2%) than only CRAM (Acc = 88.4%) where no scale information is utilized.

Model Name	Inductive Bias	Only CRAM	ACAM
ViT-Large	Positional (Pos.)	86.31 ± 0.2	87.26 ± 0.3
DeIT-Base	Positional (Pos.)	76.81 ± 0.8	76.96 ± 0.3
SWIN (1x1)	CNN-like	86.44 ± 0.8	86.72 ± 0.6
ViT-Base (Dino)	Pos. + Invariance	76.5 ± 0.2	77.2 ± 0.1

Table 3: Performance on various ViTs on CUB200 using only CRAM and ACAM. We observe that ViT architectures with CNN-like inductive biases show smaller improvements using ACAM and have comparable performance for both - ACAM and CRAM.

ViT Backbone Ablations.

Table 3 lists the prediction performance of DeIT-Base, SWIN 1x1, and ViT-Base (Dino), variants on CUB200 averaged over three seeds. We observe that ACAM outperforms CRAM on models with either a missing Positional or CNN-like inductive bias (DeIT, SWIN, ViT-Base (Dino)). This observation is expected as ACAM provides explainability which combines both Positional and CNN-like scale invariant inductive biases. Note that on SWIN, which contains pre-encoded CNN-like inductive biases, ACAM is on par with CRAM. This observation reaffirms the motivation of our approach - incorporating multiple inductive biases in the explainability module provides better explanations. We compare the quality of explanations for random test set images across ViT architectures in Appendix.

Overhead of Explanations: We also provide the overhead of the additional modules as a percentage of model parameters (Appendix). In most cases, the models augmented with CRAM consist of $\approx 2\%$ additional parameters than just the backbones. There is a negligible increase in the training and inference times.

4.6 Discussion

Figure 6 shows two examples of correctly classified images from CUB200 and one from KITS. The first row (Ground Truth) represents the ground-truth human annotations of the concepts. The second and third rows represent the explanations produced using models trained using only CRAM and ACAM on the ViT-Base backbone, respectively. We observe that ACAM can better capture regions ‘missed’ by only CRAM - the brown edge of wings in the first sample and beak shape in the second as compared to ground truth. All the pixels of the cysts in the kidney image are better captured by ACAM as compared to CRAM. (Appendix)

Robustness to transformations. We also report the qualitative performance of ACAM in small transformations in Figure 7 - rotation, random cropping, and zoom where we observe that ACAM is more robust to minor transformations.

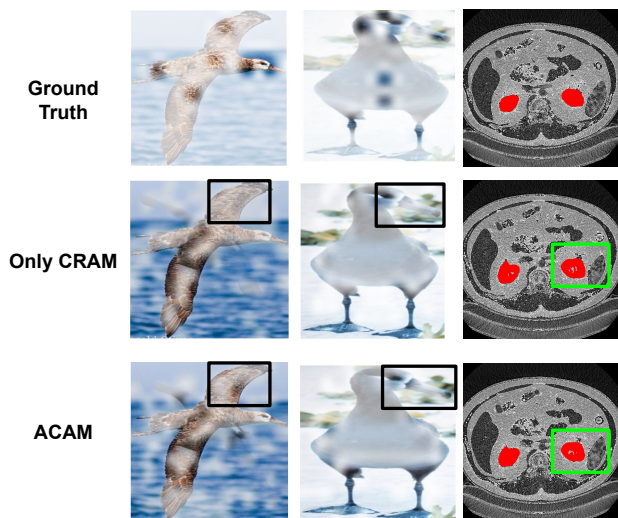


Figure 6: Visualizing concept attention scores over two samples from test set of CUB200 and one sample from KITS. We highlight the area of interest with a bounding box. (LEFT) CRAM captures the brown front and back edge of wings better than utilizing only CRAM (i.e., assigns higher attention weights). (CENTER) CRAM captures the annotations over the beak (tip) and eyes better than CRAM. (RIGHT) CRAM captures the cysts annotation much more accurately as CRAM ignores some inner patches.

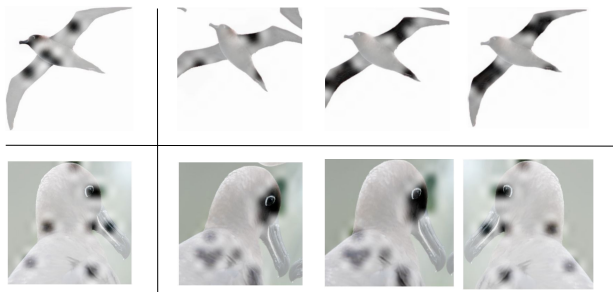


Figure 7: Robustness of concept explanations generated by CRAM with transformations applied to select test images. Row-1 shows explanation maps on random rotations and crops across the center. Row-2 shows explanation maps on random flips and rotations.

Intervention Awareness. Lastly, we show that ACAM supports interventions in case of wrong prediction. (Appendix)

5 Conclusion

In this paper, we propose Attention-based Concept Alignment Module (ACAM), a concept-based explainability module that utilizes attention to align concepts and representations. ACAM captures concepts across multiple scales using a Multi-scale Encoding Module and composes effective multiscale concept-patch relationships through a Multi-scale Feature Interaction Module. Finally, composite representations are aligned with concepts using a Concept-Representation Alignment Module. Quantitative and qualitative results demonstrate superior performance over existing methods on multiple ViT backbones. We hope our work helps in designing robust concept-based explainability modules for large-scale DNNs.

References

- Rishabh Agarwal, Levi Melnick, Nicholas Frosst, Xuezhou Zhang, Ben Lengerich, Rich Caruana, and Geoffrey E Hinton. Neural additive models: Interpretable machine learning with neural nets. *Advances in neural information processing systems*, 34:4699–4711, 2021.
- David Alvarez Melis and Tommi Jaakkola. Towards robust interpretability with self-explaining neural networks. *Advances in neural information processing systems*, 31, 2018.
- Angelika Ando, Spyros Gidaris, Andrei Bursuc, Gilles Puy, Alexandre Boulch, and Renaud Marlet. Rangevit: Towards vision transformers for 3d semantic segmentation in autonomous driving. In *Proceedings of the IEEE/CVF Conference on Computer Vision and Pattern Recognition*, pages 5240–5250, 2023.
- Sara Atito, Muhammad Awais, and Josef Kittler. Sit: Self-supervised vision transformer. *arXiv preprint arXiv:2104.03602*, 2021.
- Rishi Bommasani, Drew A Hudson, Ehsan Adeli, Russ Altman, Simran Arora, Sydney von Arx, Michael S Bernstein, Jeannette Bohg, Antoine Bosselut, Emma Brunskill, et al. On the opportunities and risks of foundation models. *arXiv preprint arXiv:2108.07258*, 2021.
- Mathilde Caron, Hugo Touvron, Ishan Misra, Hervé Jégou, Julien Mairal, Piotr Bojanowski, and Armand Joulin. Emerging properties in self-supervised vision transformers. In *Proceedings of the IEEE/CVF international conference on computer vision*, pages 9650–9660, 2021.
- Chaofan Chen, Oscar Li, Daniel Tao, Alina Barnett, Cynthia Rudin, and Jonathan K Su. This looks like that: deep learning for interpretable image recognition. *Advances in neural information processing systems*, 32, 2019.
- Zhe Chen, Yuchen Duan, Wenhai Wang, Junjun He, Tong Lu, Jifeng Dai, and Yu Qiao. Vision transformer adapter for dense predictions. *arXiv preprint arXiv:2205.08534*, 2022.
- Shaveta Dargan, Munish Kumar, Maruthi Rohit Ayyagari, and Gulshan Kumar. A survey of deep learning and its applications: a new paradigm to machine learning. *Archives of Computational Methods in Engineering*, 27:1071–1092, 2020.
- Jacob Devlin, Ming-Wei Chang, Kenton Lee, and Kristina Toutanova. Bert: Pre-training of deep bidirectional transformers for language understanding. *arXiv preprint arXiv:1810.04805*, 2018.
- Jiqian Dong, Sikai Chen, Shuya Zong, Tiantian Chen, and Samuel Labi. Image transformer for explainable autonomous driving system. In *2021 IEEE International Intelligent Transportation Systems Conference (ITSC)*, pages 2732–2737. IEEE, 2021.
- Alexey Dosovitskiy, Lucas Beyer, Alexander Kolesnikov, Dirk Weissenborn, Xiaohua Zhai, Thomas Unterthiner, Mostafa Dehghani, Matthias Minderer, Georg Heigold, Sylvain Gelly, et al. An image is worth 16x16 words: Transformers for image recognition at scale. In *International Conference on Learning Representations*, 2020.
- Ali Farhadi, Ian Endres, Derek Hoiem, and David Forsyth. Describing objects by their attributes. In *2009 IEEE conference on computer vision and pattern recognition*, pages 1778–1785. IEEE, 2009.
- Iason Gabriel. Artificial intelligence, values, and alignment. *Minds and machines*, 30(3):411–437, 2020.
- Amirata Ghorbani and James Zou. Data shapley: Equitable valuation of data for machine learning. In *International Conference on Machine Learning*, pages 2242–2251. PMLR, 2019.
- Yuan Gong, Yu-An Chung, and James Glass. Ast: Audio spectrogram transformer. *arXiv preprint arXiv:2104.01778*, 2021.
- Benjamin Graham, Alaaeldin El-Nouby, Hugo Touvron, Pierre Stock, Armand Joulin, Hervé Jégou, and Matthijs Douze. Levit: a vision transformer in convnet’s clothing for faster inference. In *Proceedings of the IEEE/CVF international conference on computer vision*, pages 12259–12269, 2021.
- Nicholas Heller, Fabian Isensee, Dasha Trofimova, Resha Tejpaul, Zhongchen Zhao, Huai Chen, Lisheng Wang, Alex Golts, Daniel Khapun, Daniel Shats, Yoel Shoshan, Flora Gilboa-Solomon, Yasmeen George, Xi Yang, Jianpeng Zhang, Jing Zhang, Yong Xia, Mengran Wu, Zhiyang Liu, Ed Walczak, Sean McSweeney, Ranveer Vasdev, Chris Hornung, Rafat Solaiman, Jamee Schoepfoerster, Bailey Abernathy, David Wu, Safa Abdulkadir, Ben Byun, Justice Spriggs, Griffin Struyk, Alexandra Austin, Ben Simpson, Michael Hagstrom, Sierra Virnig, John French, Nitin Venkatesh, Sarah Chan, Keenan Moore, Anna Jacobsen, Susan Austin, Mark Austin, Subodh Regmi, Nikolaos Papanikolopoulos, and Christopher Weight. The kits21 challenge: Automatic segmentation of kidneys, renal tumors, and renal cysts in corticomedullary-phase ct, 2023.
- Tom Heskes, Evi Sijben, Ioan Gabriel Bucur, and Tom Claassen. Causal shapley values: Exploiting causal knowledge to explain individual predictions of complex models. *Advances in neural information processing systems*, 33:4778–4789, 2020.
- Jeya Vikranth Jeyakumar, Joseph Noor, Yu-Hsi Cheng, Luis Garcia, and Mani Srivastava. How can i explain this to you? an empirical study of deep neural network explanation methods. *Advances in Neural Information Processing Systems*, 2020.
- Been Kim, Martin Wattenberg, Justin Gilmer, Carrie Cai, James Wexler, Fernanda Viegas, et al. Interpretability beyond feature attribution: Quantitative testing with concept activation vectors (tcav). In *International conference on machine learning*, pages 2668–2677. PMLR, 2018.
- Pang Wei Koh and Percy Liang. Understanding black-box predictions via influence functions. In *International Conference on Machine Learning*. PMLR, 2017.
- Pang Wei Koh, Thao Nguyen, Yew Siang Tang, Stephen Mussmann, Emma Pierson, Been Kim, and Percy Liang. Concept bottleneck models. In *International Conference on Machine Learning*, pages 5338–5348. PMLR, 2020.

- Oscar Li, Hao Liu, Chaofan Chen, and Cynthia Rudin. Deep learning for case-based reasoning through prototypes: A neural network that explains its predictions. In *Proceedings of the AAAI Conference on Artificial Intelligence*, volume 32, 2018.
- Xuhong Li, Haoyi Xiong, Xingjian Li, Xuanyu Wu, Xiao Zhang, Ji Liu, Jiang Bian, and Dejing Dou. Interpretable deep learning: Interpretation, interpretability, trustworthiness, and beyond. *Knowledge and Information Systems*, 64(12):3197–3234, 2022.
- Tsung-Yi Lin, Piotr Dollár, Ross Girshick, Kaiming He, Bharath Hariharan, and Serge Belongie. Feature pyramid networks for object detection. In *Proceedings of the IEEE conference on computer vision and pattern recognition*, pages 2117–2125, 2017.
- Ze Liu, Yutong Lin, Yue Cao, Han Hu, Yixuan Wei, Zheng Zhang, Stephen Lin, and Baining Guo. Swin transformer: Hierarchical vision transformer using shifted windows. In *Proceedings of the IEEE/CVF international conference on computer vision*, pages 10012–10022, 2021.
- Matthew O’Shaughnessy, Gregory Canal, Marissa Connor, Mark Davenport, and Christopher Rozell. Generative causal explanations of black-box classifiers. *Advances in Neural Information Processing Systems*, 2020.
- Tejaswini Pedapati, Avinash Balakrishnan, Karthikeyan Shanmugam, and Amit Dhurandhar. Learning global transparent models consistent with local contrastive explanations. *Advances in Neural Information Processing Systems*, 33, 2020.
- Maithra Raghu, Thomas Unterthiner, Simon Kornblith, Chiyuan Zhang, and Alexey Dosovitskiy. Do vision transformers see like convolutional neural networks? *Advances in Neural Information Processing Systems*, 34:12116–12128, 2021.
- Marco Tulio Ribeiro, Sameer Singh, and Carlos Guestrin. Why should i trust you?: Explaining the predictions of any classifier. In *Proceedings of the 22nd ACM SIGKDD international conference on knowledge discovery and data mining*, 2016.
- Mattia Rigotti, Christoph Miksovics, Ioana Giurgiu, Thomas Gschwind, and Paolo Scotton. Attention-based interpretability with concept transformers. In *International Conference on Learning Representations*, 2021.
- Connor Shorten, Taghi M Khoshgoftaar, and Borko Furht. Deep learning applications for covid-19. *Journal of big Data*, 8(1):1–54, 2021.
- Sanchit Sinha, Mengdi Huai, Jianhui Sun, and Aidong Zhang. Understanding and enhancing robustness of concept-based models. In *Proceedings of the AAAI Conference on Artificial Intelligence*, volume 37, pages 15127–15135, 2023.
- Sanchit Sinha, Guangzhi Xiong, and Aidong Zhang. Colidr: Concept learning using aggregated disentangled representations. In *Proceedings of the 30th ACM SIGKDD Conference on Knowledge Discovery and Data Mining*, pages 2699–2710, 2024.
- Mukund Sundararajan, Ankur Taly, and Qiqi Yan. Axiomatic attribution for deep networks. In *International conference on machine learning*, pages 3319–3328. PMLR, 2017.
- Hugo Touvron, Matthieu Cord, Matthijs Douze, Francisco Massa, Alexandre Sablayrolles, and Hervé Jégou. Training data-efficient image transformers & distillation through attention. In *International conference on machine learning*, pages 10347–10357. PMLR, 2021.
- Shikhar Tuli, Ishita Dasgupta, Erin Grant, and Thomas L Griffiths. Are convolutional neural networks or transformers more like human vision? *arXiv preprint arXiv:2105.07197*, 2021.
- Ashish Vaswani, Noam Shazeer, Niki Parmar, Jakob Uszkoreit, Llion Jones, Aidan N Gomez, Łukasz Kaiser, and Illia Polosukhin. Attention is all you need. *Advances in neural information processing systems*, 30, 2017.
- Catherine Wah, Steve Branson, Peter Welinder, Pietro Perona, and Serge Belongie. The caltech-ucsd birds-200-2011 dataset. 2011.
- Bowen Wang, Liangzhi Li, Yuta Nakashima, and Hajime Nagahara. Learning bottleneck concepts in image classification. In *Proceedings of the IEEE/CVF conference on computer vision and pattern recognition*, pages 10962–10971, 2023.
- Yongqin Xian, Christoph H Lampert, Bernt Schiele, and Zeynep Akata. Zero-shot learning—a comprehensive evaluation of the good, the bad and the ugly. *IEEE transactions on pattern analysis and machine intelligence*, 41(9):2251–2265, 2018.
- Yufei Xu, Qiming Zhang, Jing Zhang, and Dacheng Tao. Vi-tae: Vision transformer advanced by exploring intrinsic inductive bias. *Advances in neural information processing systems*, 34:28522–28535, 2021.
- Li Xu, Xin Yan, Weiyue Ding, and Zechao Liu. Attribution rollout: a new way to interpret visual transformer. *Journal of Ambient Intelligence and Humanized Computing*, 14(1):163–173, 2023.
- Xizhou Zhu, Weijie Su, Lewei Lu, Bin Li, Xiaogang Wang, and Jifeng Dai. Deformable detr: Deformable transformers for end-to-end object detection. *arXiv preprint arXiv:2010.04159*, 2020.

A Appendix

The Appendix is organized as follows:

- Implementation Details
- Effect of Model Type
- Overhead of explainability modules
- Visual comparison across ViT architectures
- Robustness Analysis
- Additional Results on Pascal dataset
- Additional Results using ACAM
- Intervention on Test Datasets

A.1 Implementation Details

ViT Backbone. We set the patch size to correspond to 16x16 pixels. Each image is resized to (224,224), hence a patch sequence is $(224/16, 224/16) = (14,14)$. We further flatten patches and utilize pre-trained positional embeddings. Following Rigotti *et al.* [2021], we append the $\langle \text{CLS} \rangle$ token to the patch sequence after positional embeddings as it is designed to encapsulate global semantics. This results in an input sequence of length of $196+1 = 197$ tokens. The internal embedding size (dim) of ViT is 1024.

MSE Module. We utilize three different scales in the Multi-scale Encoding Module, i.e., $S = 3$. We utilize the scales - 1/8, 1/16 and 1/32. This corresponds to the scale-aware vector \mathbf{c} composed of sizes: $c_1 = 1024$, $c_2 = 196$ and $c_3 = 16$, making the size of \mathbf{c} be 1029. The first convolution block consists of three convolution blocks with the batch norm and ReLU activations followed by the Max pooling operation. The following convolution blocks consist of a single convolution layer of kernel size=3 and stride=2, as well as the batch norm and ReLU activations.

DMSF Module. We utilize Multi-scale Deformable Attention [Zhu *et al.*, 2020]. We utilize 16 attention heads and four reference points, along with layer norms for each key, query, and value vector. Note that the output from the ViT backbone is appended with the $\langle \text{CLS} \rangle$ token. We strip the $\langle \text{CLS} \rangle$ token before passing through the DMSF module and append it to the output. The initialization value of \mathbf{I} is set as 0.01. The value of ψ is tunable and set as 1 for CUB, 2 for Concept-MNIST and 0.5 for AWA2.

CRAM. We utilize the same embedding dimensions, i.e., $dim = 1024$ for Key, Query and Value vectors. The number of attention heads is set as 2 for both global and spatial concept attention matrices.

Training Details. We train each dataset and backbone for 50 epochs with early stopping. The maximum learning rate is set at $5e-5$ with a linear warmup for the first 10 epochs followed by Cosine decay. Note that ViT training is negatively affected by state-less optimizers - as a consequence we use AdamW with $1e-3$ weight decay. The weight of the explanation loss is set at 1.0. The batch size is 16 for each dataset with mixed precision (16-bit default) optimization.

A.2 Effect of Model Type

Note that CRAM in our method is similar to Rigotti *et al.* [2021]. However, we amend the module to work for various

ViT architectures. The performance on the models compared in Rigotti *et al.* [2021] are on-par.

Types of inductive bias. In this section, we first discuss the types of inductive biases in various ViT architectures. Inductive bias plays an important role in determining the characteristics of the learned embeddings from the ViT architecture. Note that the standard ViT architecture only properly encodes intra-patch relationships which can be thought of as a positional-only inductive bias. SWIN on the other hand, significantly differs from standard ViTs and only contains CNN-like operations through a shifted window implementation - making the inductive biases equivalent to CNNs. Finally, in addition to the primary inductive biases, self-supervised learning techniques also encode a transformation invariance inductive bias as in Dino. DeIT [4] is a similar architecture to ViT with a data-efficient training methodology that also encodes positional inductive biases. We compare the performance against two CNN-only approaches, ST-CNN and MA-CNN Rigotti *et al.* [2021] as well in Table 4 on the CUB200 dataset. We observe ACAM outperforms all architectures.

NOTE: SWIN (1x1) is an improved version of the SWIN baseline where the final patch embedding is passed through a 1x1 convolution layer. We utilize the updated version in all the experiments in the paper.

Model Name	Inductive Bias	Only CRAM	ACAM
ST-CNN	CNN-like	82.01 ± 0.01	82.56 ± 0.01
MA-CNN	CNN-like	82.84 ± 0.03	83.32 ± 0.01
ViT-Large	Positional (Pos.)	86.31 ± 0.2	87.26 ± 0.3
DeIT-Base	Positional (Pos.)	76.81 ± 0.8	76.96 ± 0.3
SWIN (1x1)	CNN-like	86.44 ± 0.8	86.72 ± 0.6
ViT-Base (Dino)	Pos. + Invariance	76.5 ± 0.2	77.2 ± 0.1

Table 4: Performance on various ViT architectures on the CUB200 dataset using only CRAM and ACAM.

A.3 Overhead of Explanations

Table 5 lists the percentage of parameters in the standard Feed Forward Network (FFN), CRAM, and ACAM modules when used as the classifier head as a percentage of total model parameters. CRAM utilizes a modestly higher number of parameters as compared to FFN while ACAM (with the MSE and DMSF modules) introduces slightly more parameters than CRAM. Overall, the number of additional parameters remains under 3% of total model parameters. We can conclude that both ACAM and CRAM provide good explainability-efficiency tradeoffs.

Model Name	# Params	FFN	CRAM	ACAM
ViT-Base	86M	<1%	2%	2.4%
ViT-Large	307M	<1%	$\leq 1\%$	$\leq 1\%$
DeIT-Base	86M	<1%	2%	2.5%
SWIN	88M	<1%	2%	2.2%
ViT-Base (Dino)	86M	<1%	2%	2.4%

Table 5: Percentage of additional parameters introduced by specific classifier heads of various ViT architectures. CRAM and ACAM offer improved explainability at a fraction of the additional parameter cost.

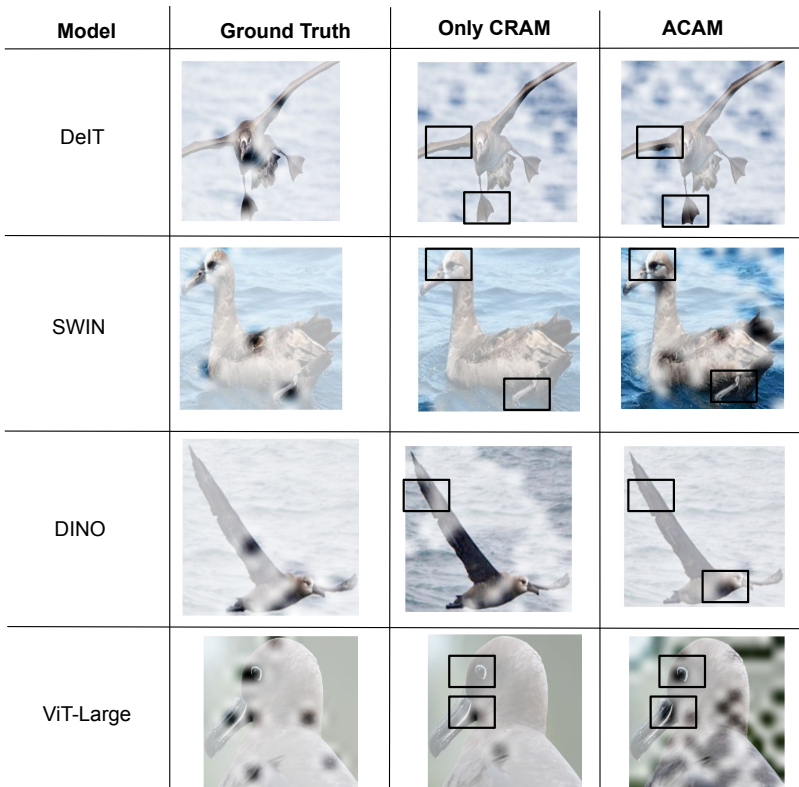


Figure 8: Comparison of explanation visualizations across different ViT architectures. The first column denotes the model architecture. Selected samples from the test set correctly classified by the model are represented in the second, third and fourth columns. The second column represents manually annotated ground truth (color) overlaid on the image. The third and fourth columns show the attention map of the CRAM and ACAM methods. The bounding boxes are areas of interest where ACAM captures detailed explanations not captured by CRAM.

A.4 Visual Comparison across ViT Architectures

Figure 8 shows some correctly classified examples from the CUB200 dataset. We compare random test set images across the four ViT architectures overlaid by the attention explanations. We observe that CRAM fails to capture sufficient concept annotations (compared to ground truth) while ACAM captures the concept annotations well. The bounding boxes (in black) are areas of interest where ACAM outperforms CRAM. Note that we utilize the same setting for background suppression as in Rigotti *et al.* [2021] for a fair comparison - which results in a few additional background pixels being identified as important.

A.5 Robustness Analysis

In addition, we demonstrate the robustness of our approach to transformations applied to the test images in Figure 10. The images in the first column are the ground-truth concept annotations. The first row shows the concept explanations identified on the images with rotation and crop transformations. We observe that ACAM can correctly identify the front and back portions of the wing as concepts. Similarly, Row-2 shows concepts identified under rotation and flip transformations. Once again ACAM can identify the correct concept annotations like the eyes and beak areas.

A.6 Additional Results on Pascal Dataset

We report additional results on the Pascal dataset - concept loss and prediction performance over different values of ψ . Note that Pascal dataset has crude annotations of concepts making concept-learning noisy. Table 6 shows the effect of a feed-forward network (FFN), CRAM and ACAM. Note that the backbone ViT architecture utilized is the ViT-Large and concept errors are the MSE loss. We observe that both CRAM and ACAM perform on par with both prediction and concept errors.

Class. Head	Spatial Wt. (ψ)	Concept Error	Accuracy (%)
FFN	-	-	81.3
CRAM	0	0.089	81.9
	0.1	0.091	80.4
	1	0.088	81.9
ACAM	10	0.083	81.7

Table 6: Results on the Pascal dataset with classifier heads as a feed-forward network (FFN), CRAM, and ACAM on the ViT-Large backbone. We observe that ACAM and CRAM perform on par.

A.7 Additional Visual Results using ACAM

Figure 11 demonstrate additional results as compared to ground-truth concept annotations for correctly from the

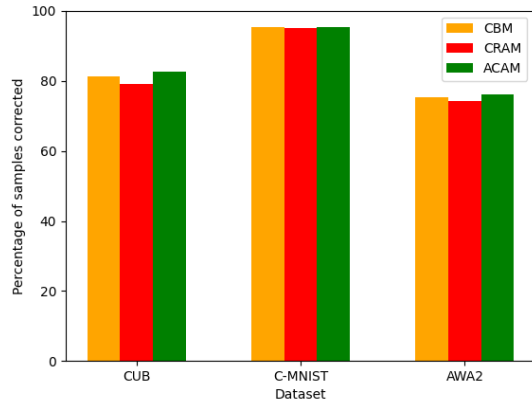


Figure 9: Test-time Intervention on datasets - CUB, MNIST (prediction) and AWA2 using CBMs (Orange), CRAM (Red) and ACAM (Green).

CUB200 dataset. Figure 12 incorrectly classified samples. For the correctly classified samples in Figure 11 report the verbose concepts subdivided into spatial and global categories.

A.8 Intervention on Test Datasets

The most important property of a human-in-the-loop system is the ability to intervene and ‘correct’ the incorrect predictions. We demonstrate the interventions on the concepts for all datasets - MNIST (prediction), CUB, and AWA2 for CRAM and ACAM (Figure 9). We compare the success rate with CBMs. The percentage of incorrectly classified samples corrected after intervention is represented in the y-axis. We observe that intervening on ACAM module beats both CRAM and CBM. Note that we can only intervene on GLObal Concepts for all datasets, i.e., C_{Global} . Surprisingly, the CRAM in itself underperforms on CBMs

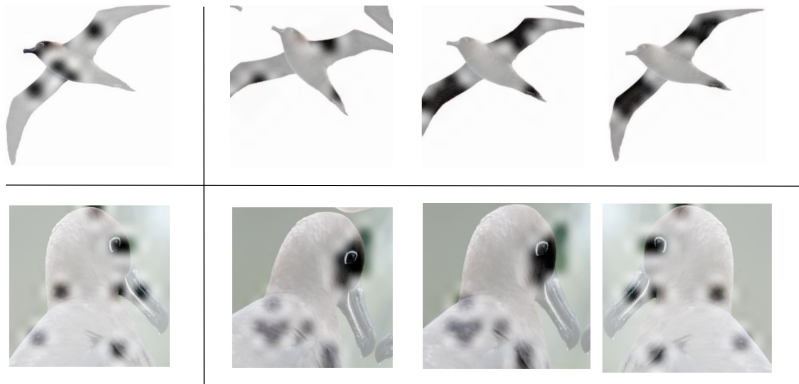


Figure 10: Robustness of concept explanations generated by ACAM with transformations applied to select test images. Row-1 shows explanation maps on random rotations and crops across the center. Row-2 shows explanation maps on random flips and rotations across the center. The identified concept explanations are consistent implying the efficacy of our approach.

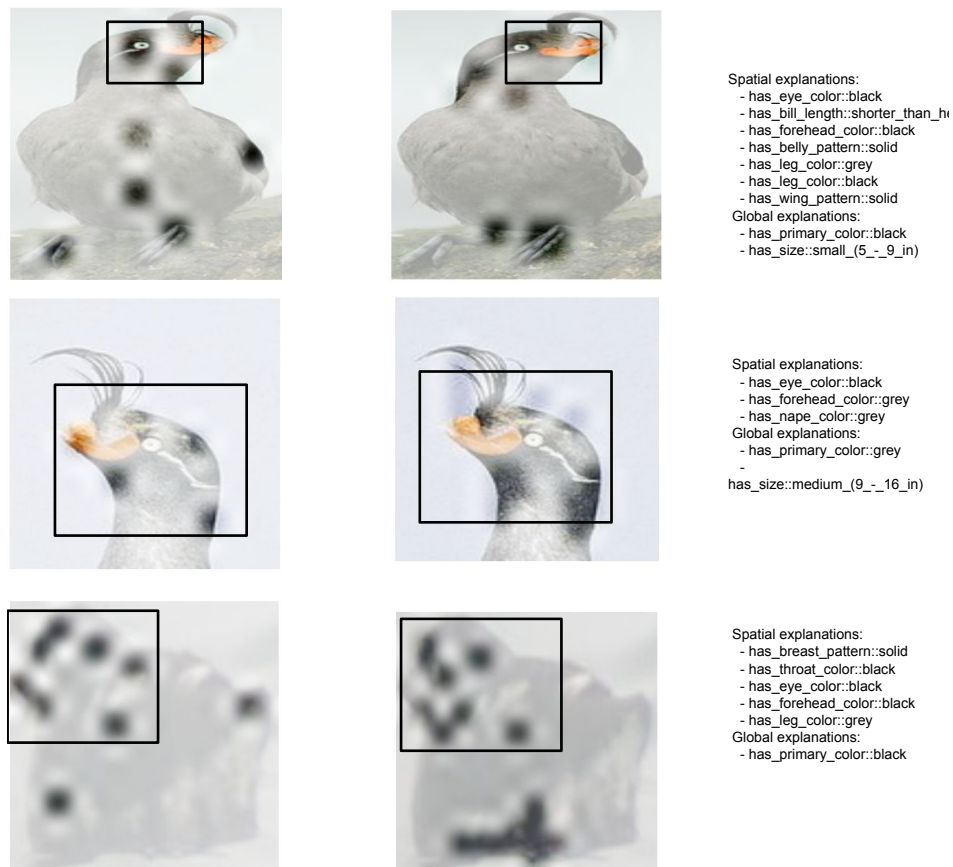


Figure 11: A few more results using ACAM on 3 randomly chosen, correctly classified test images from the CUB200 dataset along with the correctly classified concepts.

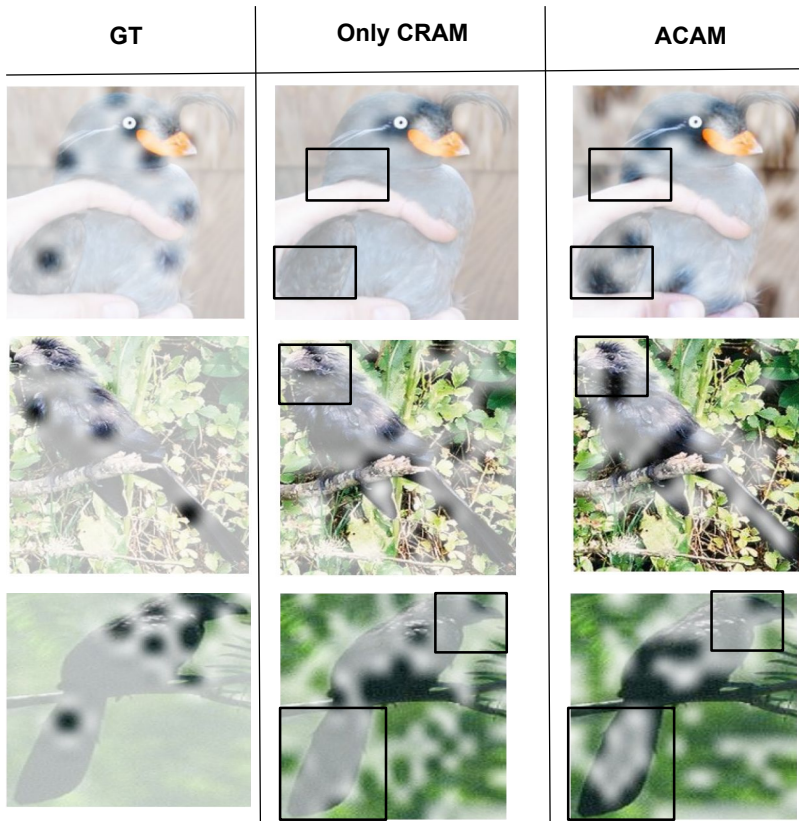


Figure 12: A few more results comparing CRAM and ACAM generated concept explanations on 3 randomly chosen, wrongly classified test images from the CUB200 dataset. Note that even when the images are classified incorrectly, ACAM learns more accurate concept maps. In all the images, we mark the area of interest through a black bounding box. In Row-1, ACAM is successfully able to capture the Nape and Wing concepts missed by only the CRAM module. In Row-2, ACAM identifies the head and under-eyes concepts better than CRAM. Finally, in Row-3, ACAM identifies the head and tail concepts missed by CRAM.